Infrared Multiple Photon Dissociation Spectroscopy of Protonated Cyameluric Acid

Walter E Olmedo, Liliana Jimenez, Andrés Cruz-Ortiz, Philippe Maître, Gustavo Pino, Maximiliano Rossa

Infrared Multiple Photon Dissociation Spectroscopy of Protonated Cyameluric Acid

Walter E. Olmedo,[a),b),c)] *Liliana B. Jiménez,*[a),d)] *Andrés F. Cruz-Ortiz,*[a),b),c)] *Philippe Maitre,*[e)] *Gustavo A. Pino,*[a),b),c)] *and Maximiliano Rossa*[a),b),c),*]

[a)] INFIQC (CONICET – Universidad Nacional de Córdoba), Ciudad Universitaria, X5000HUA Córdoba, Argentina

[b)] Dpto. de Fisicoquímica, Facultad de Ciencias Químicas, Universidad Nacional de Córdoba, Ciudad Universitaria, X5000HUA Córdoba, Argentina

[c)] Centro Láser de Ciencias Moleculares, Universidad Nacional de Córdoba, Ciudad Universitaria, X5000HUA Córdoba, Argentina

[d)] Dpto. de Química Orgánica, Facultad de Ciencias Químicas, Universidad Nacional de Córdoba, Ciudad Universitaria, X5000HUA Córdoba, Argentina

[e)] Université Paris-Saclay, CNRS, Institut de Chimie Physique, 91405, Orsay, France

Corresponding author

[*] E-mail: mrossa@fcq.unc.edu.ar (M. Rossa)

KEYWORDS

IRMPD / Cyameluric acid / *s*-Heptazine derivative / Electrospray ionization / Mass spectrometry / Ion spectroscopy / Density functional theory calculations

ABSTRACT

The present study reports the first structural characterization of protonated cyameluric acid ($[CA+H]^+$) in the gas phase, which paves the road for prospective bottom-up research on the condensed-phase chemistry of CA in protonated form. A number of $[CA+H]^+$ keto-enol isomers can *a priori* be produced, as a result of protonation on available N and O positions of precursor neutral CA tautomers, yet *ab initio* computations predict different, reduced $[CA+H]^+$ isomer populations to dominate the solution and gas phases that are involved in the ion generation process (*i.e.,* electrospray ionization). Infrared multiple photon dissociation spectra were recorded in the 990-1900 and 3300-3650 cm^{-1} regions, and compared with theoretical [B3LYP/6-311++G(d,p)] IR absorption spectra of several $[CA+H]^+$ isomers, finding a satisfactory agreement for the most stable monohydroxy form in the gas-phase, $[1358a]^+$, yet contribution of its nearly isoenergetic OH rotamer, $[1358b]^+$, cannot be dismissed. This is indicative for the occurrence of $[CA+H]^+$ isomer interconversion reactions, assisted by protic solvent molecules, during their transfer into the gas phase. The results suggest that available O positions on neutral CA are energetically favored protonation sites in the gas phase.

1. INTRODUCTION

Cyameluric acid (CA) is an *s*-heptazine (tri-*s*-triazine) derivative, characterized by the aromatic tricyclic C_6N_7 unit, and formally featuring substitution of the H atoms at the three C–H positions by OH groups.[1] Liebig and Henneberg originally reported the synthesis of CA, and its tripotassium (cyamelurate) salt in the middle of the 19th century,[2,3,4] though Pauling *et al.* in 1937 were the first postulating the existence of a "cyameluric nucleus" (C_6N_7) to describe the motif of three fused *s*-triazine rings.[5] Ever since, a number of experimental studies on CA in the solid state has confirmed such hypothesis, on the basis of IR spectroscopic data analysis,[6] and of structure elucidation via NMR spectroscopy and X-ray powder diffraction,[7] while solution of crystal structure of CA hydrate $C_6N_7O_3H_3.3H_2O$, points to the same direction.[8]

A remarkable feature of neutral CA is that, disregarding the orientation of its OH groups, it can give rise to seventeen keto-enol tautomers.[1,9,10] The favored tautomeric form in the solid state was the subject of controversy since the IR study by Finkel'shtein and Spridonova,[6] until different crystal structures finally showed that a trioxo tautomer 258 (see Scheme 1 for nomenclature), which features the three H atoms bound to peripheral nitrogen atoms, is the most stable.[7,8]

The relative stability of CA tautomers in the gas phase and in solution has received less attention, and the most comprehensive studies so far involved theoretical investigations through density functional theory (DFT) of the corresponding stable structures and energetics.[9,11,12] The 258 form was predicted to be the most stable tautomer in the gas phase, and its tautomerization to high energy-lying 136, 146, and 147 forms by means of endoergic, unimolecular proton transfer (PT) reactions was shown to have associated activation barriers higher than 150

kJ/mol.[11] These energy barriers were found to be lowered by more than 100 kJ/mol through assistance of either water and methanol molecules to the corresponding PT reactions.[12]

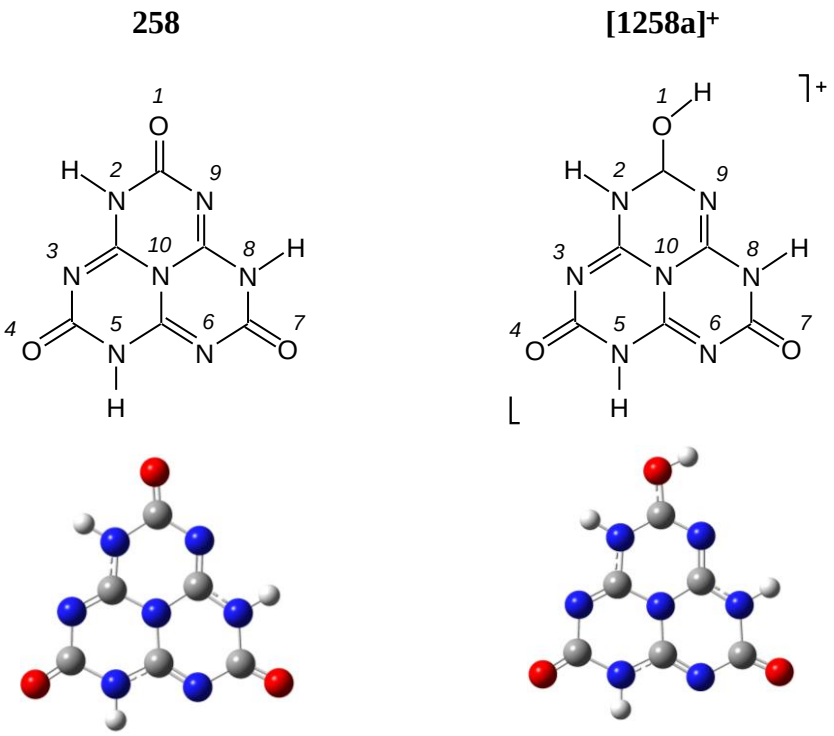

Scheme 1. Nomenclature for isomers of CA in neutral (left) and protonated (right) forms (based on that used for CA by Alkorta *et al.*, *ARKIVOC* **2004**, *4*, 130–136). For $[CA+H]^+$ rotamers of a given OH group, the more (less) stable conformer is indicated by an 'a' ('b') label. The optimized theoretical structures [B3LYP/6-311++G(d,p)] for 258 and $[1258a]^+$ are also shown in the lower row.

In this context, it should be emphasized that there is a lack of structural information on protonated CA, $[CA+H]^+$, which poses a challenge from a fundamental point of view, because protonation of any particular neutral CA tautomer on its available N and O positions is possible, thereby leading to a sizeable number of keto-enol $[CA+H]^+$ isomers that can be formed, when different precursor CA tautomers are involved. In addition, gas-phase $[CA+H]^+$ can be thought as a reductionistic model system, which may provide an insight at the molecular level of the corresponding preferred protonation sites and associated energetics, without the perturbation of

solvent molecules. Realizing a first structural characterization of gaseous $[CA+H]^+$ could thus foster prospective bottom-up research, aimed at gaining fundamental understanding on the condensed-phase chemistry of CA, as well as of recently synthesized totally or partially O-linked *s*-heptazine-based polymers, especially on their photocatalytic activity towards H_2 evolution from water.[13,14,15]

The present work reports an infrared multiple photon dissociation (IRMPD) spectroscopy study of isolated protonated cyameluric acid. Structural information on such species is obtained by comparing experimental spectra in the 990-1900 and 3300-3650 cm^{-1} regions with the theoretical IR absorption spectra of a number of $[CA+H]^+$ isomers, which formally derive from protonation of neutral CA stable tautomers. Additional electronic structure calculations on the energetics of various CA and $[CA+H]^+$ isomers in gas and solution phases, and on $[CA+H]^+$ isomer interconversion reactions were performed to elucidate the most probable CA precursors of gaseous $[CA+H]^+$ species, which are responsible for the IRMPD spectra.

2. EXPERIMENTAL AND COMPUTATIONAL METHODS

IRMPD experiments on $[CA+H]^+$ ions were performed at the Centre Laser Infrarouge d′Orsay (CLIO) on a 7T hybrid Fourier-transform Ion cyclotron resonance mass spectrometer (FT-ICR MS, Bruker Apex QE), either coupled to an infrared free-electron laser (FEL),[16] or to an optical parametric oscillator/amplifier (OPO/OPA) laser system, the latter being assisted by a CO_2 laser,[17] to record IRMPD spectra in the 990-1900 and 3300-3650 cm^{-1} regions, respectively.

The synthesis of pure cyameluric acid from polymeric melon was performed following procedures reported previously,[8] and it is described in Section S1 (Supplementary Material -SM-) along with the associated characterization (Figures S1-4). Gas-phase $[CA+H]^+$ species were

produced in an electrospray ionization (ESI) source from a solution of cyameluric acid with a concentration of $1x10^{-4}$ M and using a water/methanol 50/50 mixture as solvent. The precursor ions, featuring a majority of $[CA+H]^+$, were accumulated (during 500 ms) in the hexapole ion trap of the instrument, where they were collisionally thermalized (to near room temperature -RT-) using a flow of high-purity Ar buffer gas,[18] and subsequently pulse-extracted towards the ICR cell. No traces of a complex between $[CA+H]^+$ and one water molecule ($[CA+H]^+\_H_2O$), and of a proton-bound dimer, *i.e.*, $[CA+H+CA]^+$, were detected prior to mass selection in the ICR cell (Figure S5). The $[CA+H]^+$ ions (*m*/*z* 222.037) were sequentially mass-selected in the ICR cell and irradiated by the IR radiation delivered by either the FEL or the OPO/OPA+CO_2 laser combination.

In the case of FEL irradiation, $[CA+H]^+$ ions were irradiated for 300 ms. The spectral bandwidth of FEL is ~ 10-20 cm^{-1} for ν = 1000-1900 cm^{-1}. As described elsewhere,[17] in the alternative irradiation scheme an OPO/OPA laser system (FWHM = 3-4 cm^{-1} bandwidth; LaserVision), pumped by a non-seeded Nd:YAG laser (1064 nm, 25 Hz repetition rate, 4-6 ns pulse duration; Innolas Spitlight 600), was used in combination with a broadband CO_2 laser, which was run in a pulsed mode. A 25 ms long CO_2 pulse followed each OPO/OPA pulse, delayed each other by ~1 μs. Using the OPO/OPA+CO_2 laser combination, the irradiation time of $[CA+H]^+$ was set to 250 ms.

Upon resonant vibrational excitation, IRMPD of the $[CA+H]^+$ ions produced a single fragment with *m*/*z* 180.015 (Figure S4, SM). At each laser wavelength, the abundances of the parent (I_{parent}) and photofragment ($I_{fragment}$) ions were recorded, and the IRMPD spectra were obtained by plotting the photodissociation efficiency $Eff = -\ln(I_{parent}/(I_{parent}+\Sigma I_{fragment}))$, as a function of the laser wavenumber. Wavelength calibration of the FEL IRMPD spectrum was

performed at the data treatment stage by reference to an IR absorption spectrum of a polystyrene film, which had been monitored online during the FEL scan while recording the $[CA+H]^+$ *tandem* mass spectrum.[19] In the case of the OPO/OPA IRMPD spectrum, an off-line calibration of the output wavenumber of the OPO/OPA laser, based on the IR absorption spectrum of water vapor,[20] was used to wavelength-correct the $[CA+H]^+$ IRMPD spectrum during data treatment.

A theoretical exploration of the potential energy surfaces for the isolated CA and $[CA+H]^+$ species was performed using density functional theory at the B3LYP level, along with the 6-311++G(d,p) basis sets for all atoms. In the case of CA, the geometries of nine stable tautomers were optimized and characterized by their harmonic vibrational frequencies. For $[CA+H]^+$, twenty five isomers were optimized starting from initial guess geometries, for which a variety of possible protonation sites for the CA tautomers were considered. The theoretical IR spectra of $[CA+H]^+$ isomers in the 990-1900 and 3300-3650 cm^{-1} ranges were determined using harmonic vibrational frequencies scaled by factors of 0.9688 (as recommended elsewhere[21] for similar levels of theory as used in this study) and 0.955 (as previously used[22] in the N–H/O–H stretching region), respectively. To facilitate comparisons between measured IRMPD and theoretical IR spectra, each calculated frequency was convoluted assuming a gaussian profile with associated widths (FWHM) of 20 and 10 cm^{-1} in the 990-1900 and 3300-3650 cm^{-1} ranges, respectively.

For both CA and $[CA+H]^+$ species, screening effects of the solvent (water and methanol) on the corresponding structures were accounted for by the Dielectric Polarizable Continuum model at the B3LYP/6-311++G(d,p) level.

For isolated CA and $[CA+H]^+$, and for some of these in solution, the relative total energies (E_R), including zero-point energy (ZPE) corrections, and the relative standard Gibbs

free energies at 298 K ($\Delta G_{298\ K}$) were calculated. Relative stabilities for CA in the gas phase and in aqueous solution, were also determined from single point energy calculations using the MP2 method and the 6-311++G(d,p) basis sets, based on the geometries optimized at the B3LYP/6-311++G(d,p) level. In this MP2(Full)/6-311++G(d,p)//B3LYP/6-311++G(d,p) approach, the vibrational frequencies computed at the B3LYP/6-311++G(d,p) level were used to derive ZPE and thermal (298 K) corrections to $\Delta G_{298\ K}$.

Transition state (TS) structures for conversion between pairs of $[CA+H]^+$ isomers via intramolecular 1,3 proton transfer were also computed at the B3LYP/6-311++G(d,p) level, and the corresponding structures were characterized by vibrational analysis (one imaginary frequency). The minima connected by a given TS structure were confirmed by intrinsic reaction coordinate calculations. All of the calculations were performed using the Gaussian 09 suite of programs.[23]

3. RESULTS

The IRMPD spectra of $[CA+H]^+$ in the 990-1900 and 3300-3650 cm^{-1} ranges are shown in Figure 1, and their assignment to specific $[CA+H]^+$ isomers in the gas phase first required a theoretical exploration of the precursor keto-enol CA tautomers, both in the gas phase and in solution (water or methanol). The resulting stable structures of 9 out of 17 tautomers of isolated CA, and the corresponding values for E_R and $\Delta G_{298\ K}$ are shown in Figure S6 and Table S1 (SM), respectively. These species were chosen to encompass a wide range of energies, up to ~ 146 kJ/mol, which allows to compare the theoretical level used in this work with those of two previous reports.[9,11]

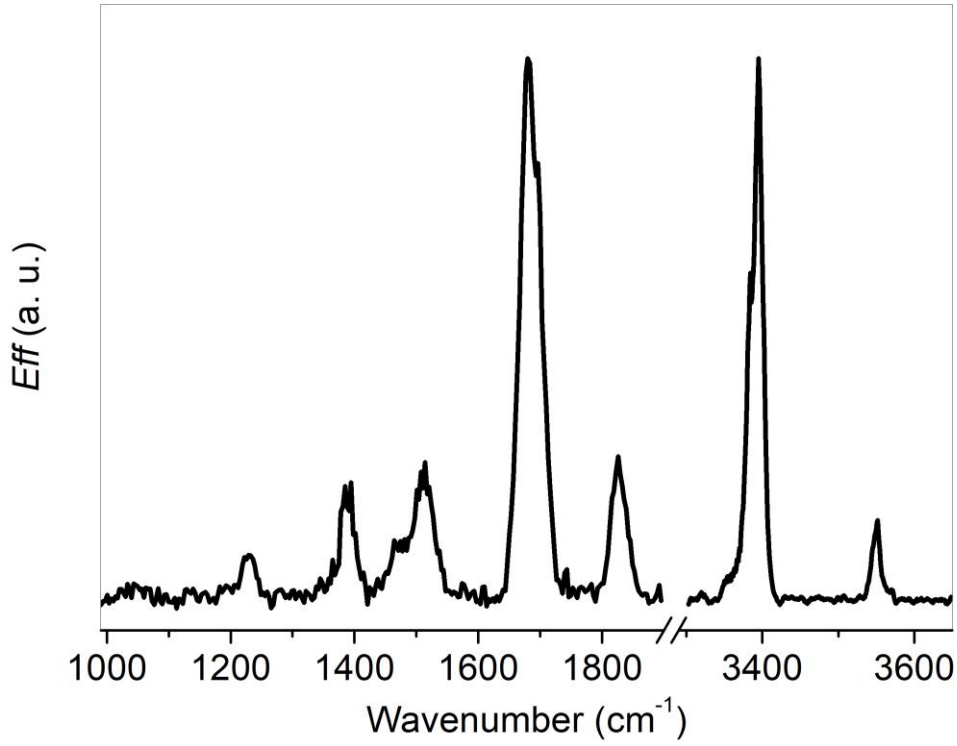

Figure 1. IRMPD spectra of $[CA+H]^+$ ions. For the sake of comparison, each spectrum has been normalized to its own maximum photodissociation efficiency.

The presently computed energy order follows that obtained at the B3LYP/6-31G(d) level by Alkorta *et al.*,[9] who studied all 17 CA tautomers. Relative energies of the 258, 136, 146, and 147 structures here are in agreement with those calculated by Liang *et al.* at the B3LYP/6-31++G(d,p) level.[11] The present DFT results for the five tautomers lying within 75 kJ/mol above the lowest energy structure (Table S1), lead to the same order of stability than MP2(Full)/6-311++G(d,p)//B3LYP/6-311++G(d,p) computations (Table S2; SM), and to E_R and $\Delta G_{298\ K}$ values that are higher than those derived from the MP2 approach by a variable amount, in the range of 1-27 %.

D-PCM calculations were also performed on the five lowest-lying CA tautomers considered here. It is found by DFT that the stability order does not change with respect to the one for isolated species, and that E_R and $\Delta G_{298\ K}$ values are barely affected (within 0.4 kJ/mol) by the identity of the solvent considered, either water or methanol (Table S1). The same general trends are derived from the MP2 approach in the gas phase and in aqueous solution (Table S2). Under the assumption of equilibrium conditions at RT in the initial (water/methanol) solution, D-PCM calculations consistently show that the population of the trioxo 258 form should be significantly favored, by about two orders of magnitude over that of the second most stable 259 tautomer.

Given the satisfactory agreement found between the energetics derived from different approaches, i.e., computation time-saving DFT and post-Hartree-Fock MP2, the former was chosen to treat the $[CA+H]^+$ species.

On the basis of CA tautomers shown in Fig. S6, a comprehensive computation of gas-phase $[CA+H]^+$ structures was performed, which led to the finding of 25 stable forms (Figure S7), named following the nomenclature for neutral species (Scheme 1). Table 1 lists the values of E_R, $\Delta G_{298\ K}$, and Boltzmann population distributions for $[CA+H]^+$ species lying at gas-phase relative energies below 46 kJ/mol, and the corresponding results of D-PCM calculations performed in water are also included. A complete list of such properties for all 25 $[CA+H]^+$ isomers in the gas phase can be found in Table S3 (SM), which additionally presents D-PCM results in both water and methanol for some selected structures.

Table 1. Computed E_R, $\Delta G_{298\ K}$, and Boltzmann population distributions (n; derived from $\Delta G_{298\ K}$) of $[CA+H]^+$ isomers. Values for E_R and $\Delta G_{298\ K}$ are in kJ/mol.

Tautomer	Gas phase	H_2O (D-PCM)

	E_R	$\Delta G_{298\,K}$	n	E_R	$\Delta G_{298\,K}$	n
[1358a]$^+$	0.0	0.0	1	1.5	3.1	$3x10^{-1}$
[1358b]$^+$	1.3	1.3	0.6	1.7	2.8	$3x10^{-1}$
[1458a]$^+$	30.2	31.2	$3x10^{-6}$	43.3	44.6	$2x10^{-8}$
[2368]$^+$	32.6	30.7	$4x10^{-6}$	0.0	0.0	1
[1258a]$^+$	38.6	38.2	$2x10^{-7}$	25.1	26.3	$2x10^{-5}$
[2358]$^+$	45.9	43.9	$2x10^{-8}$	7.8	8.3	$4x10^{-2}$

The theoretical results suggest that $[CA+H]^+$ isomers undergo a differential stabilization in solution phase, which results in a marked change in order of E_R with respect to that for the gas phase. Hence, $[2368]^+$ is predicted to be the most stable isomer both in water and methanol, with $[1358a]^+$ and $[1358b]^+$ being nearly isoenergetic. Instead, the latter two species are lowest-lying in the gas phase, with an energy difference of 1.3 kJ/mol, whereas $[2368]^+$ is the fourth most stable isomer lying at 32.6 kJ/mol above $[1358a]^+$. To assess the isomers responsible for the IRMPD spectra, these are compared in Figure 2 to theoretical IR spectra of $[1358a]^+$, $[1358b]^+$, and $[2368]^+$; the third most stable isomer in the gas phase, $[1458a]^+$, is included for completeness.

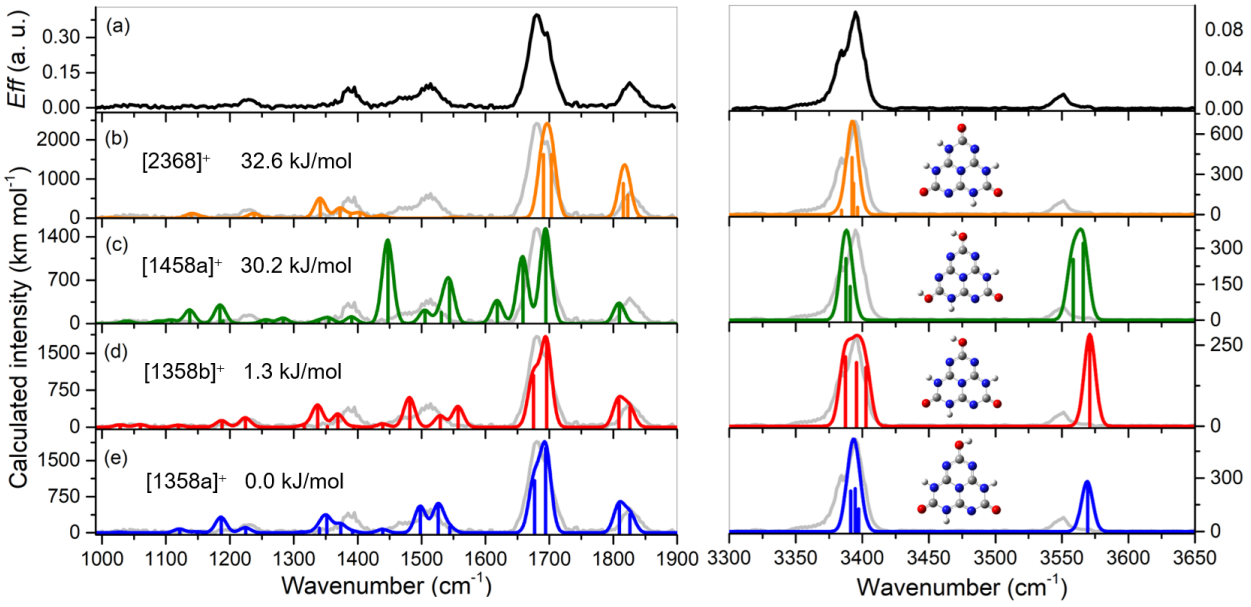

Figure 2. (a) Experimental IRMPD spectra of $[CA+H]^+$ ions. (b)-(e) Theoretical linear IR absorption spectra of the four lowest-energy isomers in the gas phase, including corresponding E_R values (taken form Table 1) and overlaid with properly scaled experimental spectra.

The most prominent features of the experimental spectra, *i.e.*, six and two IR bands in the 990-1900 and 3300-3650 cm^{-1} regions, respectively, are well reproduced by the theoretical spectra of $[1358a]^+$ and $[1358b]^+$. The agreement is generally most satisfactory for the lowest-energy $[1358a]^+$ isomer, yet the contribution of $[1358b]^+$ cannot be neglected. This is apparent in the 1600-1900 cm^{-1} range, where the shape of the intense asymmetric IRMPD band at 1680 cm^{-1} is matched by the convoluted (scaled) vibrational frequencies of 1677 and 1694 cm^{-1}, ascribable to in-plane deformations of the C_6N_7 nucleus of $[1358a]^+$, though two related modes of $[1358b]^+$ are computed nearby, at 1675 and 1696 cm^{-1}. Likewise, the relative intensity and asymmetric shape of the 1825 cm^{-1} band can be ascribed to the convolution of the stretching modes for the two free C=O groups of both $[1358a]^+$ and $[1358b]^+$, which are predicted to appear at the same vibrational frequencies of 1809 and 1826 cm^{-1}.

In the 990-1600 cm^{-1} range, a few discrepancies can be found between the observed relative band intensities and those of theoretical vibrational frequencies for $[1358a]^+$, *e.g.*, at 1186 and 1352 cm^{-1}. Considering the multiple-photon character of the IRMPD process, though, the observed band intensities should be taken with caution. Instead, whereas the computed spectrum of $[1358b]^+$ fits the experiment below 1300 cm^{-1}, the match between 1300 and 1600 cm^{-1} is unsatisfactory.

In the 3300-3650 cm^{-1} range, the most intense experimental band at 3395 cm^{-1} can be taken as diagnostic for the presence of $[1358a]^+$ and $[1358b]^+$, since the convoluted N–H stretching modes of the former fit the band near its maximum suitably, whereas the corresponding convolution of the latter account for the shoulders observed at both sides of the band peak. There is a discrepancy between the observed weaker band peak at 3550 cm^{-1}, and predicted (scaled) frequencies of 3569 and 3571 cm^{-1} due to O(1)–H stretching modes for $[1358a]^+$ and $[1358b]^+$, respectively, although a shoulder to the blue within 4 cm^{-1} of the band maximum is apparent, which could be a signature for the presence of these two isomers.

In contrast, $[2368]^+$ does not appear to contribute to the experimental spectra, *e.g.*, its linear IR spectrum lacks for the band resulting from O–H stretching at 3550 cm^{-1} [Fig. 2.(b)]. Besides, the moderately intense IRMPD feature observed between 1450 and 1550 cm^{-1} is not predicted, the dominant asymmetric band observed at 1680 cm^{-1} is predicted to be narrower, more symmetric, and shifted to the blue by 20 cm^{-1}, and the intensity of the IRMPD band peaking at 1825 cm^{-1} is predicted twice than observed. The contribution of $[1458a]^+$ can also be dismissed since three strong features are predicted between 1600 and 1700 cm^{-1}, along with a strong absorption band at 1448 cm^{-1}, which is contrary to observations [Figs. 2.(c)].

4. DISCUSSION

The results suggest that under the prevailing experimental conditions, the $[1358a]^+$ monohydroxy isomer is a major contributor to the IRMPD spectra, though the presence of the $[1358b]^+$ OH rotamer, which is partly evidenced by the shoulders on the two peaks observed in the 3300-3650 cm^{-1} range, cannot be neglected. Indeed, the IRMPD spectra can also be suitably fit by computed $[1358a]^+$:$[1358b]^+$ mixture spectra (Figure S8).

It is worth noting that the $[1358a]^+$/$[1358b]^+$ structures formally derive from protonation in the O(1) position of the 259 CA tautomer, the relative population of which should be two orders of magnitude lower than that for 258 in the initial solution. Direct protonation of 258 instead give rise to the monohydroxy $[1258a]^+$ and the trioxo $[2358a]^+$ structures (*cf.* Figs. S6 and S7), which in the gas phase lie at relative energies of ~ 39 and 46 kJ/mol, respectively, that is, well above $[1358a]^+$ (Table 1). Notwithstanding, comparison of the IRMPD spectra with the theoretical IR spectra of $[1258a]^+$ and $[2358a]^+$, suggests that these isomers are unlikely to be major contributors (Figures S9 and S10; SM).

The presence of $[1358a]^+$, and arguably of $[1358b]^+$, in the population probed by IRMPD is indicative for the occurrence of a series of exoergic isomerization reactions converting the $[1258a]^+$ isomer, which should preferentially arise by protonation of 258, into $[1358a]^+$ and $[1358b]^+$ (Scheme 2). The $[1258a]^+ \rightarrow [1358a]^+$ process requires a single intramolecular 1,3 proton transfer reaction from N(2)–H to N(3), whereas the $[1258a]^+ \rightarrow [1358b]^+$ process involves an additional rotation of the OH group around C–O(1). For the sake of completeness, the other two prospective exoergic processes, that is, $[1258a]^+ \rightarrow [2368]^+$ and $[1258a]^+ \rightarrow [1458a]^+$, are also included in Scheme 2.

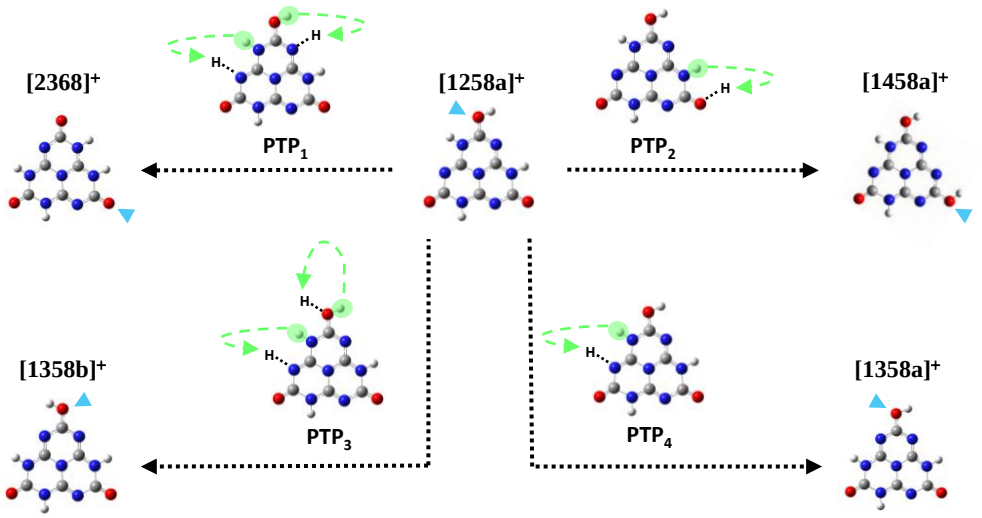

Scheme 2. The intramolecular 1,3 proton transfer processes (PTP_i; i = 1-4) involved in the formation of the $[2368]^+$, $[1458a]^+$, $[1358b]^+$, and $[1358a]^+$ isomers from $[1258a]^+$. For the sake of nomenclature clarification, the location of O(1) atom is marked with a light-blue arrow.

For isolated $[CA+H]^+$, the computed energy barriers for these proton transfer processes (PTP_i) are presented in Figure S11 (SM). In the case of PTP_4, the single PT step involved has an activation barrier of 180.0 kJ/mol. For PTP_3, the two steps required were considered to occur sequentially, thereby posing two alternative routes that are characterized by rate-limiting steps with sizeable energy barriers, namely: 192.1 kJ/mol (Route *A*) and 180.0 kJ/mol (Route *B*). In the present experiments, unimolecular PTP_3 and PTP_4 could only take place in the hexapole ion trap of the MS, where $[CA+H]^+$ ions were thermalized at near RT,[18] but given the magnitude of the energy barriers involved, the occurrence of these isomerizations is precluded at thermal energies. Similar considerations likely hold to PTP_1 and PTP_2, which were found to have large activation barriers.

The isomerization reactions in Scheme 2 can alternatively occur with the assistance of protic solvent (water or methanol) molecules, and the associated energy barriers were computed (Figure S12, SM). For PTP_4, formation of a six-membered ring transition state (*i.e.*, TS10), leads

to an activation barrier of 33.4 kJ/mol, which is lowered considerably (by −146.6 kJ/mol) with respect to the corresponding value for the unimolecular process (*cf*. Figs. S11 and S12). More importantly, TS10 lies −34.2 kJ/mol below the energy of the separated reactants $[1258a]^+ + H_2O$. The results imply that water solvent molecules can act as efficient catalysts for the $[1258a]^+ \rightarrow [1358a]^+$ process. The energy of TS10 is likely to be further reduced by the assistance of methanol molecules: This was shown in the tautomerization processes of neutral CA, for which methanol was found to decrease the associated energy barriers by ~ 4-8 kJ/mol more than water.[12]

In the water-assisted PTP_3, again two alternative routes were proposed: Whereas Route *A* necessarily requires the endoergicity of 30.2 kJ/mol to form the $[1258b]^+$ intermediate, the overall process for route *B* is found to be energy demanding by 1.3 kJ/mol, which should favor occurrence of the latter on energetic grounds. Hence, protic solvent molecules may also assist the $[1258a]^+ \rightarrow [1358b]^+$ process, accounting for the possible contribution of $[1358b]^+$ to the IRMPD spectra.

The formation of $[2368]^+$ and $[1458a]^+$ isomers from $[1258a]^+$ is also exoergic, yet all of the computed, water-assisted energies involved in PTP_1 and PTP_2 (Fig. S12) predict that their generation should be disfavored with respect to $[1358a]^+$/$[1358b]^+$ production. This supports suggestions made above that $[2368]^+$/$[1458a]^+$ are not responsible for the experimental spectra.

Although the absence of $[CA+H]^+\_H_2O$ precursor ions ensures that solvent-assisted $[CA+H]^+$ isomerization reactions do not occur in the hexapole ion trap of the MS, the theoretical results are not conclusive whether such reactions take place preferentially in the initial solution or within electrospray droplets (*i.e.*, during the transfer of $[CA+H]^+$ to the gas phase). Yet, IRMPD data suggest for a $[CA+H]^+$ population distribution to reflect the energetics of gas-phase

species in equilibrium at RT, with presence of $[1358a]^+$ and possibly of $[1358b]^+$, rather than those in solution phase, where population of $[2368]^+$ should be sizeable.

On this basis, and given the mass difference between the precursor and fragment ions of 42.022 amu, a piece of information can be obtained on the identity of the corresponding neutral elimination product, i.e., [2H,2N,C], as likely being due to carbodiimide HN=C=NH or its cyanamide tautomeric form, $N{\equiv}C{-}NH_2$.[24] Carbodiimide may be formed by rearrangement, *i.e.*, H atom migration from O(1) to N(2) or to N(9) of $[1358a]^+$ and $[1358b]^+$, respectively, prior to fragmentation. Such a rearrangement could be promoted by attractive interactions between the corresponding O(1) hydrogen atoms and the lone pairs of adjacent N(9) and N(2). Similar interactions have previously been recognized to occur in several molecular systems including DNA/RNA bases and nucleosides and their methylated derivatives, both isolated and hydrated.[25,26,27,28]

Finally, atom-charge distributions of the six most stable $[CA+H]^+$ isomers were computed through natural population analysis. The results suggest that, when a proton binds to a cyameluric acid molecule for most favored protonation sites, the proton charge delocalizes over the entire species leading to similar charges (of ~ +0.5) on the corresponding four H atoms, irrespective they are bound to N or O (Figure S13).

5. CONCLUSIONS

This first experimental study of gaseous $[CA+H]^+$ species focused on probing their structures by IRMPD spectroscopy, which posed a stringent test for such technique given the sizeable amount of isomers that could *a priori* be produced under the prevailing experimental conditions. The results suggest a dominant population of the most-stable monohydroxy isomer in

the gas phase, *i.e.*, $[1358a]^+$, although the presence of its nearly isoenergetic OH rotamer, $[1358b]^+$, cannot be dismissed. Complementary electronic structure calculations on the energetics of CA and $[CA+H]^+$ tautomers in gas and solution phases, allowed for proposing a picture for efficient production of gaseous $[1358a]^+$ and $[1358b]^+$: Starting from $[1258a]^+$ generated by direct protonation of the 258 CA form, a facile water-assisted proton transfer either in solution or within electrospray droplets may lead to $[1358a]^+$. Formation of $[1358b]^+$ requires a subsequent 180° rotation of the OH group around C–O(1) of $[1358a]^+$, which might occur before finishing the desolvation process with further assistance of solvent molecules.

The present study brings out a difference in energetically favoured protonation sites between neutral and protonated CA: Whereas the lowest-energy lying 258/259 CA tautomers feature three H atoms bound to peripheral N atoms in both gas phase and solution, the extra H^+ in gaseous $[1358a]^+$/$[1358b]^+$ binds preferentially to peripheral O atoms.

The present results will hopefully stimulate future experimental gas-phase investigations on the structure and electronic properties of *s*-heptazine-based model molecular systems, in order to build bottom-up knowledge within the current research field of their chemistry in condensed phases, particularly their photocatalytic activity for hydrogen evolution from water.

ASSOCIATED CONTENT

Supporting Information

Synthetic procedure of solid CA from melon and their characterization, including XRD and FTIR-ATR of melon, FTIR of CA, and MS/MS spectra of $[CA+H]^+$ ions produced under ESI/FT-ICR conditions before and after irradiation with FEL and OPO/OPA+CO_2 laser; MS spectra of precursor ions produced from ESI/FT-ICR; optimized structures at the B3LYP/6-311++G(d,p) level of isolated CA and $[CA+H]^+$ isomers; values for E_R, $\Delta G_{298\ K}$, and Boltzmann

population distributions of CA and $[CA+H]^+$ isomers in gas and solution (D-PCM model) phases computed both at the B3LYP/6-311++G(d,p) level, and at the MP2(Full)/6-311++G(d,p)//B3LYP/6-311++G(d,p) level for selected CA tautomers; comparison between IRMPD spectra of $[CA+H]^+$ ions and theoretical [B3LYP/6-311++G(d,p)] linear IR absorption spectra of isomers $[2358]^+$, $[1258a]^+$, and a Boltzmann-weighted mixture of $[1358a]^+$ and $[1358b]^+$; optimized structures and E_R values [B3LYP/6-311++G(d,p)] for both unimolecular and water-assisted isomerization of $[CA+H]^+$ ions; hydrogen atom-charge distributions computed by NPA of selected gas-phase $[CA+H]^+$ isomers.

ACKNOWLEDGMENTS

This work was conducted under the International Associated Laboratory LIA/LEMIR (CONICET-CNRS). Financial support from FONCyT, CONICET, SeCyT-UNC, EU Horizon 2020 Program (CALIPSOPlus and EU_FT-ICR_MS, under grant numbers 730872 and 731077, respectively), and the National FT-ICR network (FR3624 CNRS) for conducting the research, is gratefully acknowledged. W.E.O. and A.F.C.-O. acknowledge doctoral fellowships from FONCyT and CONICET, respectively. M. R. thanks to SINALA-MINCyT for funding a training stay at CLIO in 2019. The authors are grateful to Silvia Ermeninto from INTI-Córdoba for her support with the synthesis of melon, to Alejandro D. Menzaque from the Centro de Transferencia Tecnológica "Laboratorio de Caracterización de Materiales Cristalinos" (INFIQC-CONICET/UNC) for technical support with the XRD technique, and to Guillermo G. Montich (CIQUIBIC-CONICET/UNC) for collaborating in the record of FTIR-ATR spectra.

REFERENCES

(1) Schwarzer, A.; Saplinova, T.; Kroke, E. Tri-s-triazines (s-heptazines) - From a “mystery molecule” to industrially relevant carbon nitride materials. *Coord. Chem. Rev.* **2013**, *257*, 2032–2062.

(2) Liebig, J. Ueber einige Stickstoff-Verbindungen. *Ann. Pharm.* **1834**, *10*, 1-47.

(3) Henneberg, W. Ueber einige Zersetzungsproducte des Mellonkaliums. *Ann. Chem. Pharm.* **1850**, *73*, 228-255.

(4) Liebig, J. Ueber die Constitution der Mellonverbindungen. *Ann. Chem. Pharm.* **1855**, *95*, 257-282.

(5) Pauling, L.; Sturdivant, J. H. The Structure of Cyameluric Acid, Hydromelonic Acid, and Related Substances. *Proc. Natl. Acad. Sci. USA* **1937**, *23*, 615-620.

(6) Finkel’shtein, A. I.; Spiridonova, N. V. Chemical Properties and Molecular Structure of Derivatives of sym-Heptazine [1,3,4,6,7,9,9b-Heptaazaphenalene, Tri-1,3,5-Triazine]. *Russ. Chem. Rev.* **1964**, *33*, 400-405.

(7) Seyfarth, L.; Sehnert, J.; El-Gamel, N. E. A.; Milius, W.; Kroke, E.; Breu, J.; Senker, J. Structure Elucidation of Cyameluric Acid by Combining Solid-State NMR Spectroscopy, Molecular Modeling and Direct-Space Methods. *J. Mol. Struct.* **2008**, *889*, 217-228.

(8) Sattler, A.; Schnick, W. On the Question of the Tautomerism of Cyameluric Acid in the Crystal. *Z. Anorg. Allg. Chem.* **2006**, *632*, 1518-1523.

(9) Alkorta, I.; Jagerovic, N.; Elguero, J. Theoretical Study of Cyameluric Acid and Related Compounds. *ARKIVOC* **2004**, *4*, 130–136.

(10) El-Gamel, N. E. A.; Seyfarth, L.; Wagler, J.; Ehrenberg, H.; Schwarz, M.; Senker, J.; Kroke, E. The Tautomeric Forms of Cyameluric Acid Derivatives. *Chem. Eur. J.* **2007**, *13*, 1158-1173.

(11) Liang, X.; Zheng, W.; Wong, N.-B.; Li, J.; Tian, A. Theoretical Study on the Mechanism of Keto–Enol Isomerization for Cyanuric Acid and Cyameluric Acid. *THEOCHEM* **2004**, *672*, 151–159.

(12) Liang, X.; Zheng, W.; Wong, N.-B.; Shu, Y.; Tian, A. Solvent-Assisted Catalysis Mechanism on Keto–Enol Tautomerism of Cyameluric Acid. *THEOCHEM* **2005**, *732*, 127–137.

(13) Lau, V. W.-H.; Moudrakovski, I.; Botari, T.; Weinberger, S.; Mesch, M. B.; Duppel, V.; Senker, J.; Blum, V.; Lotsch, B. V. Rational Design of Carbon Nitride Photocatalysts by Identification of Cyanamide Defects as Catalytically Relevant Sites. *Nat. Commun.* **2016**, *7*, 12165.

(14) Battula, V. R.; Kumar, S.; Chauhan, D. K.; Samanta, S.; Kailasam, K. A True Oxygen-Linked Heptazine Based Polymer for Efficient Hydrogen Evolution. *Appl. Catal. B* **2019**, *244*, 313–319.

(15) Jing, L.; Xu, Y.; Zhou, M.; Deng, J.; Wei, W.; Xie, M.; Song, Y.; Xu, H.; Li, H. Novel Broad-Spectrum-Driven Oxygen-Linked Band and Porous Defect Comodified Orange Carbon Nitride for Photodegradation of Bisphenol A and 2-Mercaptobenzothiazole. *J. Hazard. Mater.* **2020**, *396*, 122659.

(16) Bakker, J. M.; Besson, T.; Lemaire, J.; Scuderi, D.; Maitre, P. Gas-Phase Structure of a π-Allyl-Palladium Complex: Efficient Infrared Spectroscopy in a 7 T Fourier Transform Mass Spectrometer. *J. Phys. Chem. A* **2007**, *111*, 13415−13424.

(17) Sinha, R. K.; Nicol, E.; Steinmetz, V.; Maitre, P. Gas Phase Structure of Micro-Hydrated $[Mn(ClO_4)]^+$ and $[Mn_2(ClO_4)_3]^+$ Ions Probed by Infrared Spectroscopy. *J. Am. Soc. Mass Spectrom.* **2010**, *21*, 758−772.

(18) Hernández, O.; Paizs, B.; Maitre, P. Rearrangement Chemistry of a_n Ions Probed by IR Spectroscopy. *Int. J. Mass Spectrom.* **2015**, *377*, 172−178.

(19) McNary, C. P.; Nei, Y.-W.; Maitre, P.; Rodgers, M. T.; Armentrout, P. B. *Phys. Chem. Chem. Phys.* **2019**, *21*, 12625−12639.

(20) The HITRAN database. https://hitran.org/ (accessed September 16, 2019).

(21) Merrick, J. P.; Moran, D.; Radom, L. An Evaluation of Harmonic Vibrational Frequency Scale Factors. *J. Phys. Chem. A* **2007**, *111*, 11683-11700.

(22) Durand, S.; Rossa, M.; Hernandez, O.; Paizs, B.; Maître, P. IR Spectroscopy of b_4 Fragment Ions of Protonated Pentapeptides in the X−H (X = C, N, O) Region. *J. Phys. Chem. A* **2013**, *117*, 2508−2516.

(23) Frisch, M. J. *et al. Gaussian 09*, Revision B.01; Gaussian Inc.: Wallingford CT, 2010.

(24) Schneider, W. C. The Structures of Cyanamide and Carbodiimide. *J. Am. Chem. Soc.* **1950**, *72*, 761-763.

(25) Salpin, J. Y.; Guillaumont, S.; Tortajada, J.; MacAleese, L.; Lemaire, J.; Maitre, P. Infrared Spectra of Protonated Uracil, Thymine and Cytosine. *ChemPhysChem* **2007**, *8*, 2235-2244.

(26) Bakker, J. M.; Sinha, R. K.; Besson, T.; Brugnara, M.; Tosi, P.; Salpin, J. Y.; Maitre, P. Tautomerism of Uracil Probed via Infrared Spectroscopy of Singly Hydrated Protonated Uracil. *J. Phys. Chem. A* **2008**, *112*, 12393-12400.

(27) Wu, R. R.; Yang, B.; Frieler, C. E.; Berden, G.; Oomens, J.; Rodgers, M. T. N3 and O2 Protonated Tautomeric Conformations of 2′-Deoxycytidine and Cytidine Coexist in the Gas Phase. *J. Phys. Chem. B* **2015**, *119*, 5773−5784.

(28) J.-Y. Salpin, V. Haldys, V. Steinmetz, E. Léon, M. Yáñez, M. M. Montero-Campillo, Protonation of Methyluracils in the Gas Phase: The Particular Case of 3-Methyluracil. *Int. J. Mass Spectrom.* **2018**, *429*, 47–55.

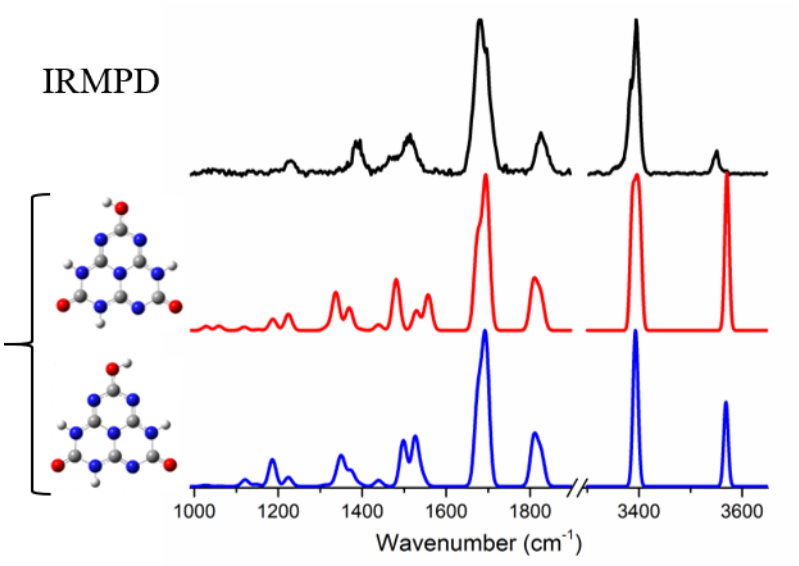

Table of Contents (TOC) Graphic